

Growth and characterization of ceria thin films and Ce-doped γ -Al₂O₃ nanowires using sol-gel techniques

This article has been downloaded from IOPscience. Please scroll down to see the full text article.

2010 Nanotechnology 21 465606

(<http://iopscience.iop.org/0957-4484/21/46/465606>)

View [the table of contents for this issue](#), or go to the [journal homepage](#) for more

Download details:

IP Address: 131.227.242.90

The article was downloaded on 30/11/2010 at 10:53

Please note that [terms and conditions apply](#).

Growth and characterization of ceria thin films and Ce-doped γ -Al₂O₃ nanowires using sol–gel techniques

S Gravani^{1,2}, K Polychronopoulou¹, V Stolojan², Q Cui³,
P N Gibson⁴, S J Hinder², Z Gu³, C C Doumanidis¹, M A Baker²
and C Rebholz¹

¹ Mechanical and Manufacturing Engineering Department, Engineering School, University of Cyprus, 1678, Nicosia, Cyprus

² Faculty of Engineering and Physical Sciences, University of Surrey, Guildford GU2 7XH, UK

³ Department of Chemical Engineering and CHN/NCOE Nanomanufacturing Center, University of Massachusetts Lowell, Lowell, MA 01854, USA

⁴ Institute for Health and Consumer Protection, Joint Research Centre of the European Commission, 21027 Ispra (VA), Italy

E-mail: M.Baker@surrey.ac.uk

Received 13 July 2010, in final form 9 September 2010

Published 26 October 2010

Online at stacks.iop.org/Nano/21/465606

Abstract

γ -Al₂O₃ is a well known catalyst support. The addition of Ce to γ -Al₂O₃ is known to beneficially retard the phase transformation of γ -Al₂O₃ to α -Al₂O₃ and stabilize the γ -pore structure. In this work, Ce-doped γ -Al₂O₃ nanowires have been prepared by a novel method employing an anodic aluminium oxide (AAO) template in a 0.01 M cerium nitrate solution, assisted by urea hydrolysis. Calcination at 500 °C for 6 h resulted in the crystallization of the Ce-doped AlOOH gel to form Ce-doped γ -Al₂O₃ nanowires. Ce³⁺ ions within the nanowires were present at a concentration of <1 at.%. On the template surface, a nanocrystalline CeO₂ thin film was deposited with a cubic fluorite structure and a crystallite size of 6–7 nm. Characterization of the nanowires and thin films was performed using scanning electron microscopy, transmission electron microscopy, electron energy loss spectroscopy, x-ray photoelectron spectroscopy and x-ray diffraction. The nanowire formation mechanism and urea hydrolysis kinetics are discussed in terms of the pH evolution during the reaction. The Ce-doped γ -Al₂O₃ nanowires are likely to find useful applications in catalysis and this novel method can be exploited further for doping alumina nanowires with other rare earth elements.

(Some figures in this article are in colour only in the electronic version)

1. Introduction

Aluminium oxide is one of the most widely used catalyst supports on an industrial scale, due to its low cost and high surface area [1]. However, the most catalytically active phases, such as γ - and η -Al₂O₃ present problems at high temperatures due to phase transformations. The transition from γ -Al₂O₃ to α -Al₂O₃, leads to a considerable reduction of the surface area, causing a degeneration of the catalytic activity [2]. Thermal stability can be enhanced by retarding

or delaying phase transitions and it has been shown that rare earth element additions, such as Ce, will not only retard the phase transformation from γ -Al₂O₃ to α -Al₂O₃, but will also stabilize the pore structure of alumina [2–4].

CeO₂ is one of the most reactive rare earth metal oxides and has been used as a promoter or support in industrial catalytic processes. Due to its high oxygen storage capacity (OSC), associated with rich oxygen vacancies and low redox potential between Ce³⁺ and Ce⁴⁺, and due to its good ion conductivity, thermal stability and strong

ultraviolet light absorption, CeO₂ has been utilized in three-way-catalysis [5, 6], solid oxide fuel cells (SOFC) [7], solar cells [8], UV blocking [9], gas sensing [10] and corrosion protection [11].

The technological properties of a catalyst strongly depend on the hydrothermal stability and texture of the support. Consequently, the specific surface area, pore size and shape and any chemical or physical modifications which result in a more stable material are of great importance. Furthermore, nanostructured materials exhibit interesting characteristics owing to their shape-specific and quantum size effects. In the case of catalyst supports for example, the high surface areas associated with one-dimensional nanostructures will always enhance adsorption and catalytic properties [12]. For this reason, to date, several reports have described the synthesis of amorphous, boehmite (AlOOH) or γ -Al₂O₃ nanostructures, which most typically involve hydrothermal treatments [13–16] or through-etching of porous alumina templates [17–19]. Surprisingly, although the beneficial effects of lanthanide additions to the thermal and structure stability of γ -Al₂O₃ have been successfully demonstrated, studies describing the synthesis of Ce-doped γ -Al₂O₃ nanowires, have not been reported for sol–gel or other solution-derived γ -Al₂O₃ nanomaterials (particles, membranes).

Here, we have employed a novel combination of a traditional sol–gel treatment with the hydrothermal ‘pore sealing’ phenomenon which occurs in anodic aluminium oxide templates. The templates are hydrothermally treated in hot water [20–22] to form AlOOH nanowires inside the template pores. However in this work, the ‘pore sealing’ occurs while treating the template in a cerium nitrate solution, which doubly serves to form AlOOH but also to incorporate Ce. Urea added in the solution increases the amount of OH[−] available for the precipitation of both cerium and aluminium hydroxides. Also, as a conventional sol–gel technique, the process allows the formation of a CeO₂ thin film. This novel synthesis method offers interesting possibilities for the formation of a selection of technologically interesting metal A doped–metal B oxide nanowires with varying compositions and structures.

2. Experimental details

2.1. Anodic aluminium oxide templates

High-purity Al sheets (99.999%, Advent Materials, 250 μ m thick) were ultrasonically cleaned in acetone for 15 min, etched in a 1 M NaOH to remove the native oxide and washed thoroughly with distilled water. The pre-treated sheets were electropolished in a mixed solution of HClO₄:CH₃CH₂OH = 1:4 (V/V) for 5 min and immediately washed with distilled water. The samples were anodized in a suitable electrolytic cell in which a 4.15 cm² surface area of the Al sheet was exposed to the electrolyte and a Pt mesh was used as a cathode. The potential was applied using a Keithley 2300 power supply interfaced with a PC, to monitor the current–time transient during the process. Anodization was performed in a vigorously stirred solution of 0.3 M H₂C₂O₄, under a constant voltage of 40 V at 25 °C for 2, 10 or 12 h. Subsequently, pore widening of the samples was carried out in a 5 vol% H₃PO₄ solution at 25 °C for 30 min.

2.2. Nanowire and thin film preparation

All chemical reagents used were analytical grade. The precursor solution contained 0.01 M cerium nitrate (Ce(NO₃)₃·6H₂O) (Sigma-Aldrich) in distilled water. Urea was added to the solution, so that the metal precursor/urea molar ratio was 1/40. A clear solution was produced, which was then heated at 90 °C while being vigorously stirred. AAO membranes were immersed into the solution for 8 h while the temperature was kept at 90 °C. The pH and temperature were measured throughout the sol–gel treatment using a Mettler Toledo pH electrode. Finally the samples were air-dried overnight and then calcinated at 500 °C, for 6 h, with an initial heating rate of 10 °C min^{−1}.

2.3. Characterization

The morphology was characterized by scanning electron microscopy (SEM) with both Tescan Vega and JEOL 7401F microscopes operated at a 30 kV incident electron beam voltage. Prior to SEM characterization, the filled template samples were etched in 1 M NaOH for 8 min and carefully washed with distilled water in order to selectively dissolve the AAO and expose the nanowires which were assembled in the template. Subsequently, both of the samples containing the nanowire and the thin film were sputter-coated with 8 nm of Au. In order to observe the morphology and the degree of agglomeration, transmission electron microscope (TEM) images were taken with a Philips CM200 TEM (LaB₆) and Hitachi 2300A STEM (Schottky), both operated at 200 kV. SEM and TEM samples were prepared by loosening the nanowires from the template by partially dissolving the AAO in 0.25 M NaOH solution, for 10 min. Then each template surface was scratched by a flat-tip tweezer and the material that was peeled from the surface was placed again in 0.25 M NaOH for 10 more minutes, to completely dissolve any Al₂O₃ remnants. The isolated nanowires were washed three times with deionized water and then ethanol, and were kept dispersed in ethanol solution for further characterization. TEM samples were prepared by drop casting a nanoparticle dispersion (in ethanol) onto copper grids coated with a Formvar and carbon film (200 mesh, SPI, West Chester, PA) for TEM characterization and on Si wafers for SEM characterization. Electron energy loss spectroscopy (EELS) was undertaken using the Gatan Imaging Filter on the TEM and a Gatan Enfina spectrometer on the STEM. Point-by-point analysis was performed in the STEM with a 2.5 Å-diameter electron beam, using Gatan’s spectrum imaging tool, with a probe convergence semi-angle of 14 and 16 mrad collection semi-angle; the energy spread of the beam was 0.8 eV FWHM. X-ray diffraction (XRD) data were recorded using an in-house developed glancing angle XRD (GAXRD) system at the European Commission’s Joint Research Centre, Ispira, Italy. The diffractometer has a laser alignment system for determination of incident angle, an instrumental resolution of about 0.2°, a solid state detector for improved signal/noise ratio, and operates with a Cu K α x-ray source (λ = 1.5418 Å). All GAXRD scans were measured at an incident angle of

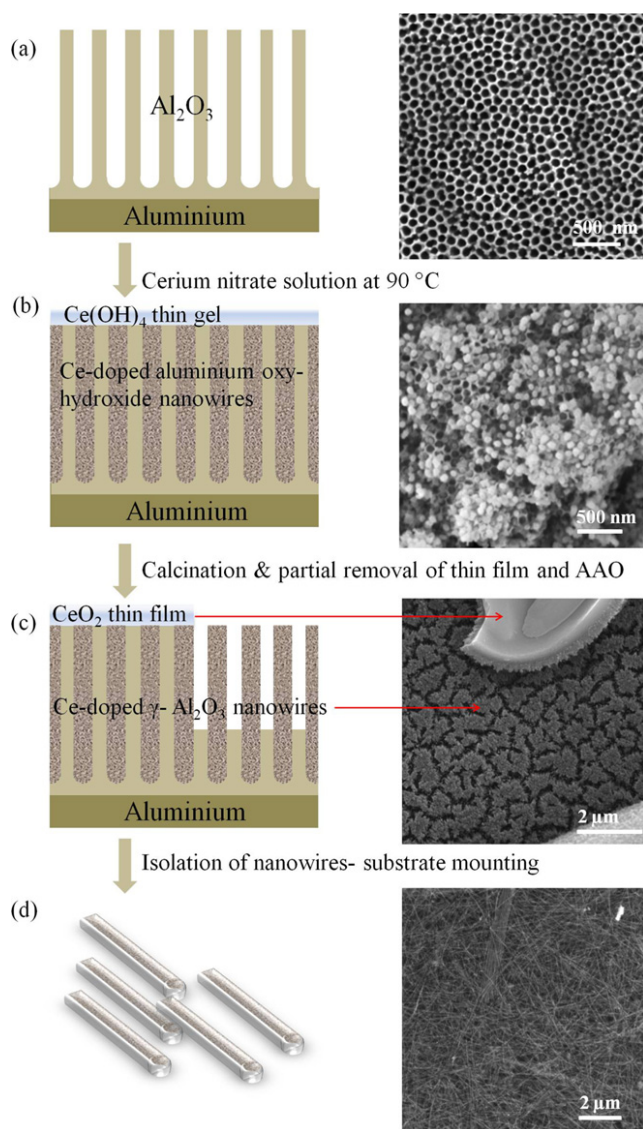


Figure 1. Schematic representation of the thin film deposition and nanowire formation paired with SEM images: (a) plan view of a typical porous alumina template; (b) filled template after the sol-gel treatment; (c) CeO₂ thin film and Ce-doped γ -Al₂O₃ nanowires following calcination at 500 °C and etching in NaOH to partially remove the AAO template; (d) free-standing nanowires on a Si wafer after detachment from the Al substrate and complete dissolution of the AAO.

1°. Crystallite grain sizes were determined using the single-line method of de Keijser, based on the least-squares fitting of broadened peaks to a pseudo-Voigt function [23]. X-ray photoelectron spectroscopy (XPS) data were recorded on a VG ESCALAB mk II, employing a non-monochromated Al K α source operated at 12 kV and 30 mA and hemispherical analyser. The binding energy was charge referenced using the C 1s hydrocarbon contamination peak at 285.0 eV. Wide scan spectra were recorded at a pass energy of 100 eV and elemental peaks at a pass energy of 20 eV. The energy resolution for the elemental narrow scans was 0.5–0.6 eV. Prior to analysis samples were etched using a 3 kV 1 μ A Ar⁺ beam for 30 s in order to reduce the surface carbon contamination.

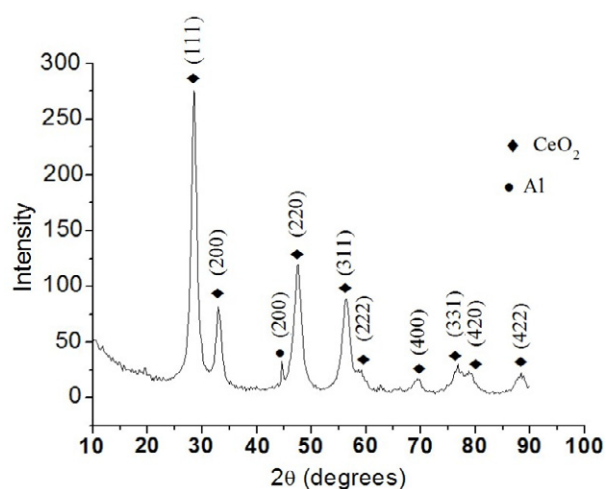


Figure 2. GAXRD pattern at 1° incident angle of CeO₂ thin film deposited by sol-gel on the AAO template.

3. Results

The in-house prepared AAO templates were examined to determine their geometrical characteristics, prior to being used in nanowire synthesis. SEM analysis indicated that a typical template is 70 μ m thick and has pores that vary between 50 and 70 nm, at a density of 4×10^{10} pores cm⁻². The process overview for the thin film and nanowire formation is summarized schematically, together with SEM micrographs from each of the different stages in figure 1. The prepared template (figure 1(a)) was treated in a temperature-controlled urea hydrolysis sol-gel method, with cerium nitrate as the precursor material. During the process, Ce-containing aluminium oxy-hydroxide precipitated inside the pores, filling them completely and causing pore sealing, as seen in figure 1(b). A Ce(OH)₄ gel was subsequently deposited, on top of the sealed AAO template. Following calcination and partial etching of the template in NaOH, the thin film and nanowires were evident (figure 1(c)). Finally, the AAO was completely dissolved in order to collect nanowires for further characterization. Figure 1(d) shows isolated nanowires mounted on a Si wafer.

3.1. Thin film

The sol-gel deposited thin film was characterized further to examine its structure. Figure 2 shows a GAXRD pattern of the CeO₂ thin film deposited on the AAO template. The sample exhibits peaks that correspond to the (111), (200), (220), (311), (222), (400), (331), (420) and (422) planes of the cubic fluorite structure (space group: *Fm*3*m*) of CeO₂, as identified from standard data (JCPDS 34-0394). The CeO₂ lattice parameter calculated from this pattern is in very close agreement (within 0.02%) with that of the JCPDS value for bulk CeO₂ ($a = 5.4113$). The crystallite size of the film was found to be \sim 6–7 nm and is close to the expected value for sol-gel materials derived at calcination temperatures of up to 700 °C [24].

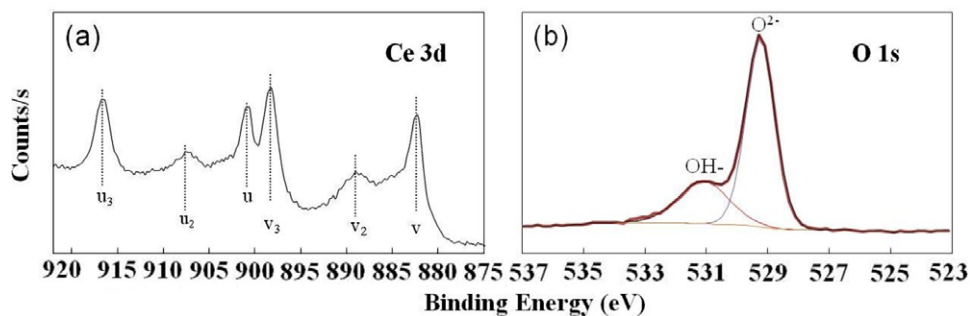


Figure 3. (a) Ce 3d and (b) O 1s XPS spectra of the sol-gel deposited CeO₂ thin film obtained after Ar⁺ etching for 30 s.

The chemical state of Ce in the thin film was also investigated by XPS. Figure 3 illustrates the XPS spectra of the deposited film obtained after argon ion etching its top surface for 30 s. From the Ce 3d core-level spectra (figure 3(a)), six Ce 3d_{5/2} binding energy peaks are identified at 882.6, 889.2, 898.6, 901.2, 907.8 and 917 eV, corresponding to v, v₂, v₃ and u, u₂, u₃ components, as reported by Ardelean *et al* [25] and Rao *et al* [26] for Ce⁴⁺. No Ce³⁺ peaks were observed. It should be noted that the binding energies are shifted to slightly higher values (0.2–0.4 eV) compared to those reported by Rao *et al* [26], as the C 1s hydrocarbon peak was referenced to 284.6 eV in the paper of Rao *et al* compared to the 285.0 eV hydrocarbon reference used in this work and that of Ardelean *et al* [25]. In the O 1s spectra (figure 3(b)), the peak splits into two separate components, of which the lower binding energy component (529.3 eV) originates from lattice O²⁻ and the higher binding energy component (531.3 eV) can be ascribed to OH⁻ groups on or near the surface of the sample [27].

3.2. Nanowires

The morphology and the structure of the synthesized nanowires were examined in detail. Figure 4 is a typical SEM image of the Ce-doped γ -Al₂O₃ nanowires which were obtained after the partial dissolution of the AAO template in NaOH. A high density of nanowires is evident, each nanowire being many microns in length. The morphological characteristics of the nanowires were more closely examined using TEM. Example TEM images of free-standing nanowires, after completely etching away the AAO template in NaOH, are shown in figures 5(a) and (b). The nanowires have a uniform thickness and structure. The high magnification image, figure 5(b), shows that the nanowire is approximately 50 nm in diameter. It has a ‘coarse’ texture and its bulk consists of apparently randomly oriented nanocrystallites. SEM and TEM characterization revealed that the nanowires were up to tens of microns in length, with diameters of 50–70 nm. Their diameter distribution is in close agreement with the pore sizes of the applied AAO template.

Compositional analysis of the nanowires was examined through EELS. Figure 6(a) shows a small group of nanowires indicated on the image as area (B) and a nanoparticle as (A). EELS analysis performed in each location revealed that the nanowires consisted largely of Al and O and that the particle

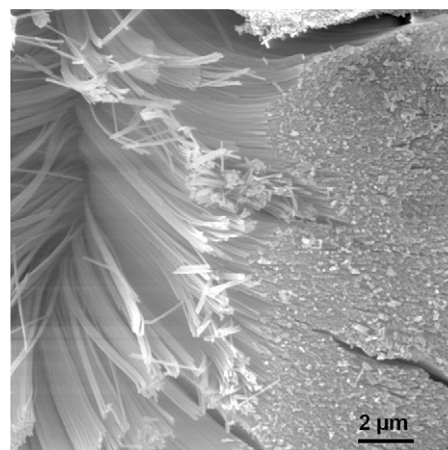


Figure 4. SEM image of high aspect ratio Ce-doped γ -Al₂O₃ nanowires after the partial removal of the AAO template.

was a CeO₂ fragment, most probably originating from the sol-gel surface layer. The EELS Ce M_{4,5} edge obtained directly from the nanoparticle is presented in figure 6(b) and represents transitions from the spin-orbit split 3d-orbital to empty states in the 4p and 4f-orbitals, with the transitions to 4f dominating due to the much higher cross-section than that of transitions to 4p. The shape is consistent with that given by Garvie and Buseck [28] and other authors [29, 30] for Ce⁴⁺ (CeO₂). The Ce⁴⁺ M₅ and M₄ edges consist of two maxima separated by 17.6 eV (indicated as A and A' in figure 6(b)), that correspond to electron transitions from the 3d_{5/2} and 3d_{3/2} respectively. The M₅ maximum has been aligned to that given by Garvie and Buseck at 884.0 eV [28]. The M₅ and M₄ peaks are further degenerated, with small satellite peaks on the high energy side (indicated as B and B' in figure 6(b)) at 889.3 and 906.5 eV respectively, assigned to crystal-field splitting. The high-resolution TEM image (figure 6(c)) shows the presence of crystallites, with a lattice fringe spacing which is consistent with that of bulk CeO₂ ($d_{111} = 3.12$ Å) and a selected area electron diffraction (SAED) pattern taken of a similar particle together with surrounding nanowires (figure 6(d)) shows reflections assignable to CeO₂. Hence, we concluded that this nanoparticle is a fragment of the CeO₂ sol-gel deposited thin film.

The crystalline nature of the nanowires was investigated by SAED and bright- and dark-field imaging. As mentioned

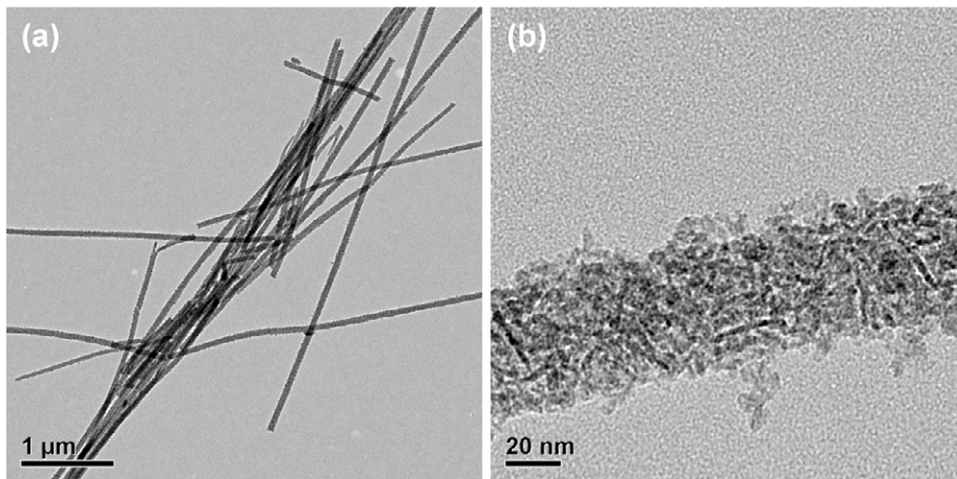


Figure 5. TEM bright-field images: (a) a bundle of nanowires; (b) high magnification image of a single nanowire.

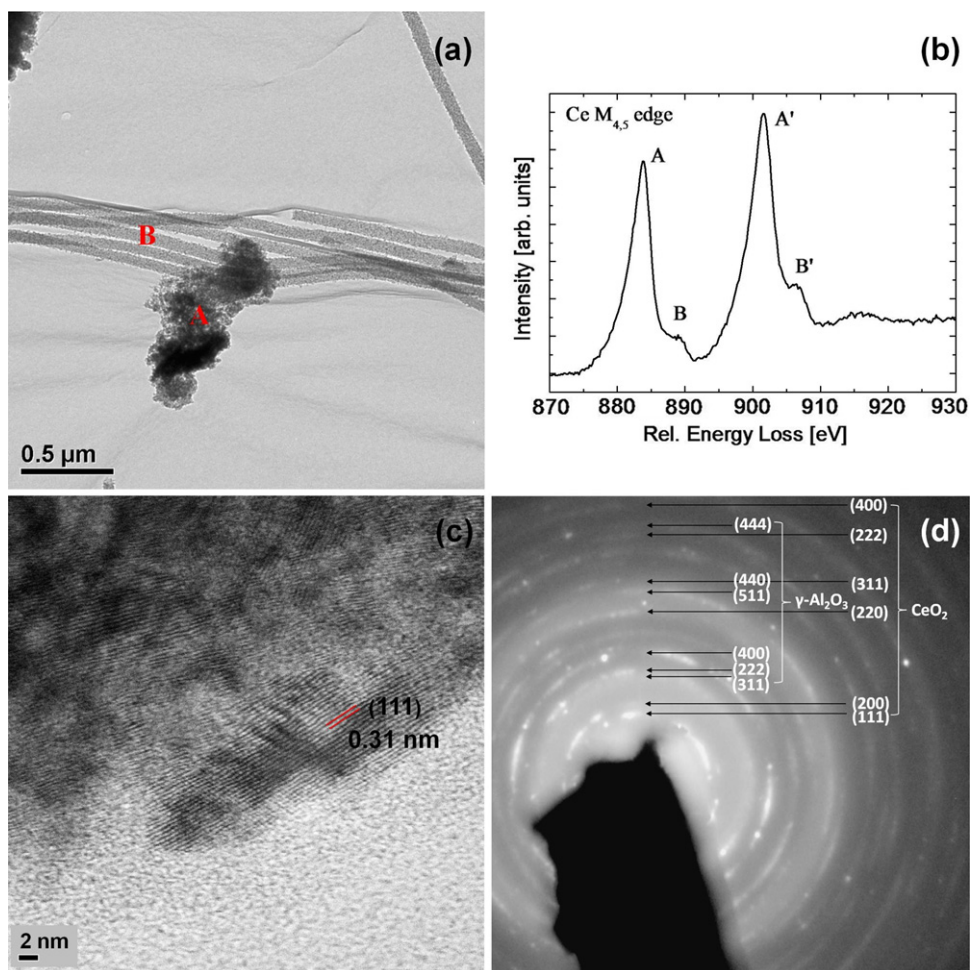


Figure 6. (a) TEM image of nanoparticle and nanowires, (b) EELS Ce $M_{4,5}$ edge spectra of nanoparticle, (c) HRTEM image of nanoparticle and (d) SAED pattern obtained from area as presented in (a).

above, figure 6(d) shows a SAED from an area containing both a CeO_2 nanoparticle and a group of nanowires. In addition to the CeO_2 reflections, other diffraction rings could be assigned to the $\gamma-Al_2O_3$ phase. (figure 6(d)). The corresponding bright- and dark-field TEM images in figure 7 clearly show the nanocrystalline nature of the nanowires, with the average

$\gamma-Al_2O_3$ grain size being 2–3 nm. The dark-field image was obtained by forming an image with the 400, 222 and 311 reflections of $\gamma-Al_2O_3$ in figure 6(d).

To obtain more detailed information on the chemical composition of the nanowires, EELS data for Al, O and Ce, were recorded by scanning the beam across two nanowires, as

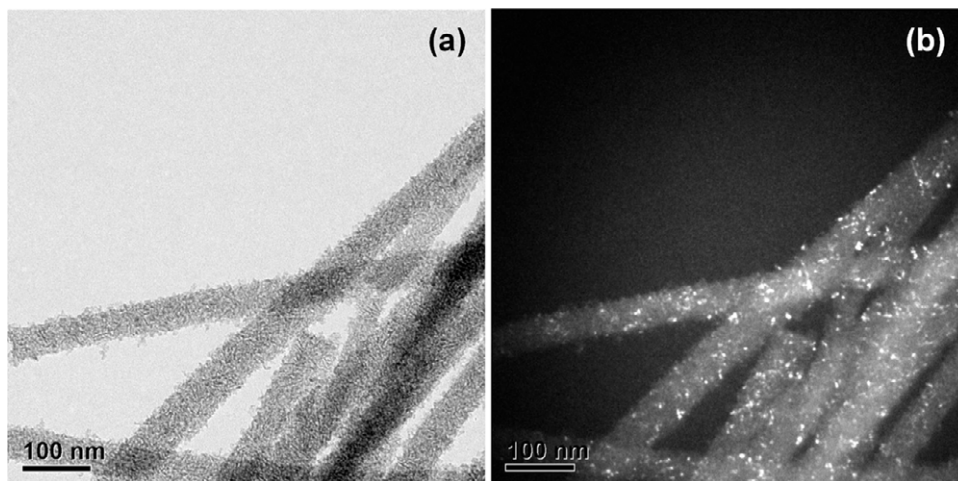


Figure 7. Bright-field (a) and dark-field (b) TEM images of nanowires.

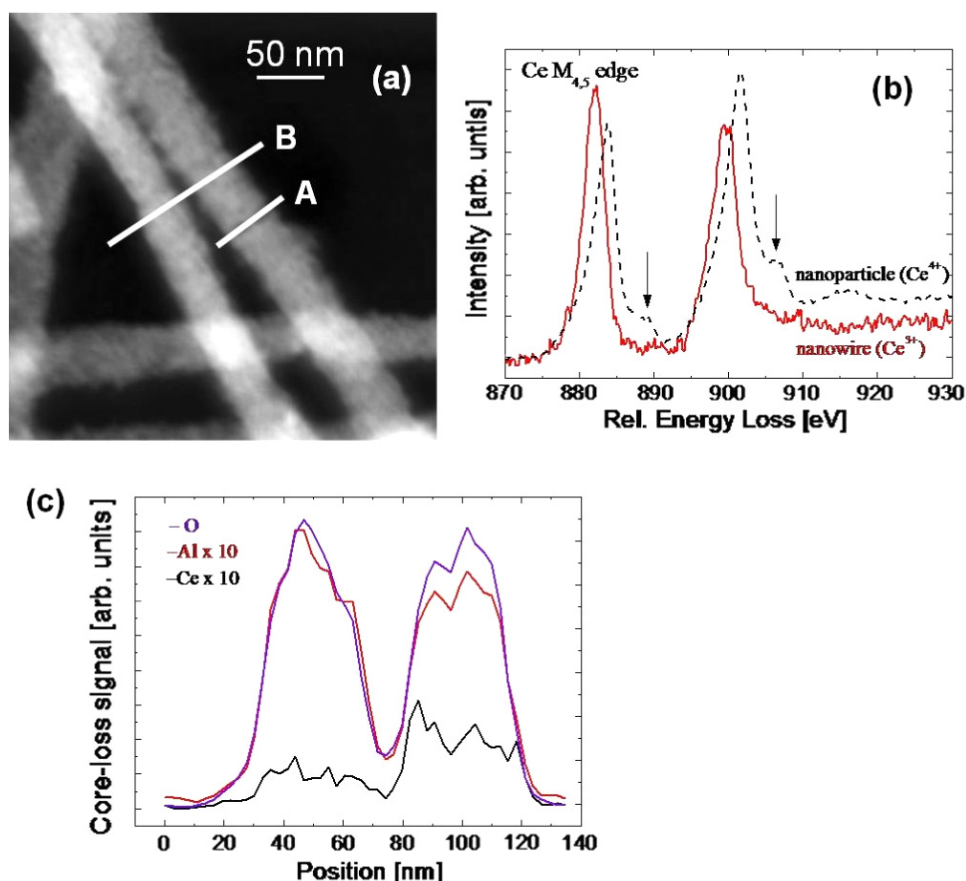


Figure 8. (a) STEM image indicating EELS linescan location; (b) comparative EELS Ce $M_{4,5}$ edge for the nanowires (solid line) and CeO_2 nanoparticle (dotted line); (c) comparative O/Al/Ce linescan intensities (displayed as core-loss signal instead of composition, due to the absence of a scattering cross-section for the Ce M-edge. The Al and Ce intensities have been multiplied by a factor of ten for presentation purposes).

shown in figure 8(a). The EELS spectra generated for each element were integrated intensities from each point on the linescan. The thickness of the wires analysed in figure 8(a) is $\sim 0.4\lambda$ (where λ is the mean free path for inelastic scattering, which for alumina is 116 nm [31]) therefore correction of the spectra for thickness artefacts is not necessary. The spectra

showed high intensity Al L-edge and O K-edge and a smaller Ce integrated M-edge signal. These high Al and O peak intensities are consistent with the identification of $\gamma-Al_2O_3$ in the SAED pattern of figure 6(d). Figure 8(b) shows the integrated Ce $M_{4,5}$ edge from a single nanowire, corresponding to linescan A in figure 8(a). The Ce $M_{4,5}$ edge shape and

peak positions are significantly different from that of Ce^{4+} described earlier for the CeO_2 nanoparticle (superimposed on figure 8(b) with a dashed line). In particular, for the nanowire, the high energy satellites (labelled B and B' in figure 6(b)) characteristic of Ce^{4+} , are no longer present. The nanowire Ce $M_{4,5}$ peak shape is consistent with that reported by Garvie and Buseck [28] for Ce^{3+} (Ce_2O_3) and again the M_5 peak maximum in figure 8(b) has been aligned with their value of 882.0 eV. In addition to the peak shape, the intensity ratio between the M_5 and M_4 edges can also be used to determine the valence state of Ce [28]. In the nanowires examined here, the M_5/M_4 ratio across the nanowire was found to be 0.80 which is comparable to the 0.82 reported value for Ce_2O_3 and for the CeO_2 nanoparticle, the M_5/M_4 ratio of 0.60 is comparable to the reported value of 0.67 for CeO_2 [28]. Electron beam damage is not the cause of this transformation [28], as acquiring several Ce M-edge spectra at the same place on several pristine nanowires did not show any significant change in the shape of the edge, but instead, simply a removal of material.

With regard to establishing the Ce content in the $\gamma\text{-Al}_2\text{O}_3$ nanowires, quantification is problematic due to the absence of a reliable EELS cross-section for the Ce M-edge. However, utilizing the EELS results from the CeO_2 nanoparticle, an experimentally determined value for Ce was evaluated. A second linescan (marked as B on figure 8(a)) was taken across two nanowires. Figure 8(c) presents the raw integrated intensities under the Al, O and Ce edges across the nanowires. The O intensity in both nanowires is similar. The Al intensity is high and Ce intensity low in the first nanowire. In the second nanowire, the Al intensity is slightly lower and Ce intensity slightly higher. This would suggest that there may be an inverse relationship between the Al and Ce intensities (possibly indicative of a substitution/exchange of Al and Ce within the nanocrystalline oxide structure), but more results would be required to confirm this. Due to the large energy-loss cross-section for the Ce M-edge, when quantified, the Ce concentration is found to be <1 at.% and the Al:O atomic ratio approximately 2:3 in both nanowires.

4. Discussion

4.1. Formation of CeO_2 thin films

The GAXRD and XPS results presented in this work have shown that a nanocrystalline CeO_2 thin film, with a cubic fluorite structure and average grain size of 6–7 nm, can be successfully deposited using a sol–gel process, employing a 0.01 M cerium nitrate solution containing urea, at a Ce:urea molar ratio of 1:40 and calcination at a temperature of 500 °C for 6 h. The cerium nitrate based sol–gel process assisted by urea reported previously used a Ce:urea molar ratio of 20 and a reaction temperature of 80 °C [32]. In this work the Ce:urea molar ratio was changed to 1:40 and the reaction temperature increased to 90–100 °C. The motivation for these changes to the previously reported process were as follows: the urea concentration was increased to raise the amount of OH^- available and increase the precipitation rate. The reaction

temperature was increased to 90–100 °C in order to maximize the hydrolysis of the increased amount of urea.

4.2. Deposition of Ce-doped $\gamma\text{-Al}_2\text{O}_3$ nanowires

From SEM, TEM and EELS analysis, it has been shown that under the same process conditions which lead to the deposition of a CeO_2 thin film on top of a porous anodic alumina template, within the template, Ce-doped $\gamma\text{-Al}_2\text{O}_3$ nanowires are formed. The nanowires were up to tens of microns in length, with diameters of 50–70 nm. The $\gamma\text{-Al}_2\text{O}_3$ grain size is approximately 2–3 nm and Ce is found to be present as Ce^{3+} ions within the nanowires, at a concentration of <1 at.%.

4.3. Sol–gel/hydrothermal based formation mechanism of the Ce-doped $\gamma\text{-Al}_2\text{O}_3$ nanowires

A cerium nitrate urea-assisted sol–gel technique has previously been applied to porous alumina templates by Wu *et al* [32], through which they obtained cubic fluorite CeO_2 nanowires. In that work, although not explicitly stated, the porous alumina layer was detached from the aluminium substrate and was subsequently etched to widen the pores and perforate the hemispherical, scalloped geometry situated at the bottom of each pore. In our work, we have utilized the geometry of substrate supported, one-side, open-ended alumina templates, in order to hydrothermally pore seal during the sol–gel process and obtain Ce-doped $\gamma\text{-Al}_2\text{O}_3$ nanowires. The proposed formation mechanism of the Ce-doped $\gamma\text{-Al}_2\text{O}_3$ nanowires is described in the following sub-sections.

4.3.1. Hydrothermal pore sealing. Porous anodic alumina is considered to be generally amorphous and have a composition which varies from that of pure Al_2O_3 [33, 34]. Both anions from the electrolyte and hydroxyl ions are incorporated into the amorphous anodic alumina structure [33]. XRD analysis of anodic films formed in a nitric acid have indicated that the amorphous alumina which forms resembles a cubic distorted $\gamma\text{-Al}_2\text{O}_3$ and hydroxyl ions are incorporated to form pseudo-boehmite (AlOOH) [34]. Hydrothermal pore sealing can occur in water, water vapour or in this case, a 0.01 M cerium nitrate:urea solution in a molar ratio of 1:40, heated and stirred at 90 °C for 8 h. Jha *et al* employed doubly distilled water and proposed that, during the hydrothermal pore sealing process, the water in the pores dissolves the amorphous alumina to form a gel which, upon saturation, precipitates as pseudo-boehmite or boehmite inside the pores [20]. In this work, the porous anodic alumina template is not treated in boiling water, but instead is undergoing a simultaneous sol–gel treatment in order to introduce Ce as well.

4.3.2. Sol–gel process. The sol–gel process involves the hydrolysis of a precursor molecule in solution to first obtain a suspension of colloidal particles (the sol) and then a gel composed of aggregate sol particles [12]. The hydrolysis of cations can be controlled by a slow release of hydroxide ions into the metal salt solution. This was achieved by the decomposition of an organic compound, in this case

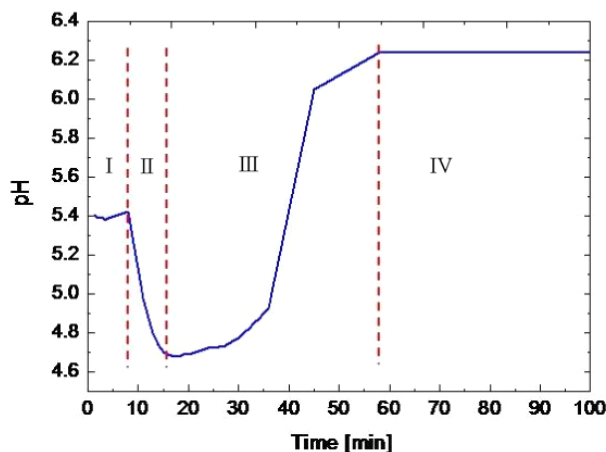


Figure 9. Evolution of pH during the hydrolysis reaction.

urea, which is a very weak Brønsted base, highly soluble in water and its hydrolysis can be controlled by varying the temperature. During the decomposition of urea, CO_3^{2-} and OH^- are produced, accompanied by an increase in the pH, leading to the precipitation of metal basic carbonates and hydroxides.

The pH increase with time, as the reaction proceeds, is indicative of the hydrolysis kinetics and is shown in figure 9. Four distinct phases can be described. In phase I, the temperature is increasing to its stable value of 90°C , the pH having a constant value of 5.4. (Reaction temperatures in the range of $90\text{--}100^\circ\text{C}$ allow the hydrolysis of urea at a high rate [35] and hence this temperature was used during the reaction to maximize precipitation.) Following stabilization at 90°C , phase II is characterized by the hydrolysis of urea and the pH dropping to low values. This is followed by a release of OH^- (phase III) in which the hydroxyl ions react immediately with (i) the template pore walls to form aquo-hydroxo complexes (intermediate species for the precipitation of aluminium hydroxide) and (ii) with the cerium cations which become incorporated into the aluminium hydroxide (evidently at small amounts). Following successful pore closure, precipitation continues and a cerium hydroxide film forms on top of the AAO template. Phase IV is characterized by a high rate of OH^- consumption (high reaction rate) and leads to a stable pH.

With regard to the kinetics of AlOOH precipitation inside the template pores during the cerium nitrate solution treatment, it should be expected that this occurs more rapidly than for conventional hydrothermal treatments in water, due to the increased amount of available OH^- which assists the reaction process, expediting the precipitation of AlOOH.

TEM and SAED analysis have confirmed that the calcination process has resulted in the precipitated AlOOH being transformed into $\gamma\text{-Al}_2\text{O}_3$. This is in agreement with previous reports that $\gamma\text{-Al}_2\text{O}_3$ phase forms upon dehydration of AlOOH at temperatures between 400 and 700°C [13, 36]. Ce^{3+} ions from the 0.01 M cerium nitrate solution have become incorporated into the nanowire structure.

4.3.3. *Formation of free-standing Ce-doped $\gamma\text{-Al}_2\text{O}_3$ nanowires.* The SEM and TEM micrographs in figures 4 and 5 show that exposure to 1 M NaOH has resulted in the porous anodic alumina being dissolved, yielding free-standing Ce-doped $\gamma\text{-Al}_2\text{O}_3$ nanowires. This is consistent with the results of Mardilovich *et al*, in which they show that $\gamma\text{-Al}_2\text{O}_3$ is much more stable to acid and base attack than amorphous alumina [38]. They propose that the presence of hydroxyl groups in the amorphous anodic alumina and specifically a structure with aluminium ions bonded to two terminal hydroxyl groups is more active in the etching process, leading to a poorer resistance to acids and bases.

4.3.4. *Schematic representation of Ce-doped $\gamma\text{-Al}_2\text{O}_3$ nanowire formation.* A schematic diagram of the different process steps in the Ce-doped $\gamma\text{-Al}_2\text{O}_3$ nanowire formation is presented in figure 10. Prepared AAO templates are immersed in the 0.01 M cerium nitrate:urea solution ($1:40$ molar ratio)—figure 10(a). Hydration of the pore walls leads to the formation of aquo-hydro complexes which upon saturation lead to the precipitation of Ce-containing aluminium oxy-hydroxide (Ce-AlOOH) which fills the pores and causes pore sealing—figure 10(b). Following, hydrothermal pore sealing, calcination at 500°C for 6 h (figure 10(c)) leads to transformation of Ce-AlOOH to Ce-doped $\gamma\text{-Al}_2\text{O}_3$ (figure 10(c)). Etching in 1 M NaOH allows the selective dissolution of the amorphous Al_2O_3 template and formation of free-standing Ce-doped $\gamma\text{-Al}_2\text{O}_3$ nanowires—figure 10(d).

4.4. Bonding of Ce in the Ce-doped $\gamma\text{-Al}_2\text{O}_3$ nanowires

The EELS results have shown that Ce is present in the nanowires as Ce^{3+} ions. It would be expected that the Ce^{3+} ions are bonding with O^{2-} ions to form Ce_2O_3 , but the exact location of the Ce^{3+} ions is not known. It might be expected that the large difference in radius between Ce^{3+} (1.034 \AA) and Al^{3+} (0.51 \AA) would not lead to direct substitution, and hence the Ce ions may be segregating to more energetically favourable grain boundary sites within the nanocrystalline $\gamma\text{-Al}_2\text{O}_3$ nanowires. However, substitution of Al^{3+} by a rare earth $3+$ ion could occur if there is a substantial rearrangement of the nearest neighbour environment to provide the necessary space. Kaplyanskii *et al* [37] have observed the successful incorporation of rare earth $3+$ ions such as Eu^{3+} , Er^{3+} , Pr^{3+} , via a sol-gel technique, in a distorted $\gamma\text{-Al}_2\text{O}_3$ lattice and after annealing above 900°C also in $\alpha\text{-Al}_2\text{O}_3$.

4.5. Further development of the sol-gel/hydrothermal pore sealing method

The described synthesis technique can be exploited further to obtain a range of technologically interesting metal A doped-metal B oxide nanowires with different compositions and structures through varying, the metal salt A (i.e. doping with other rare earth elements such as Y, La, Gd, Nd), the metal salt concentration (e.g. $1, 3, 5\text{ at.}\%$), the metal B oxide template material (e.g. titania) and also the annealing process to obtain different crystallographic forms of the metal B oxide such as δ -, θ - and $\alpha\text{-Al}_2\text{O}_3$ or anatase, brookite and rutile (TiO_2).

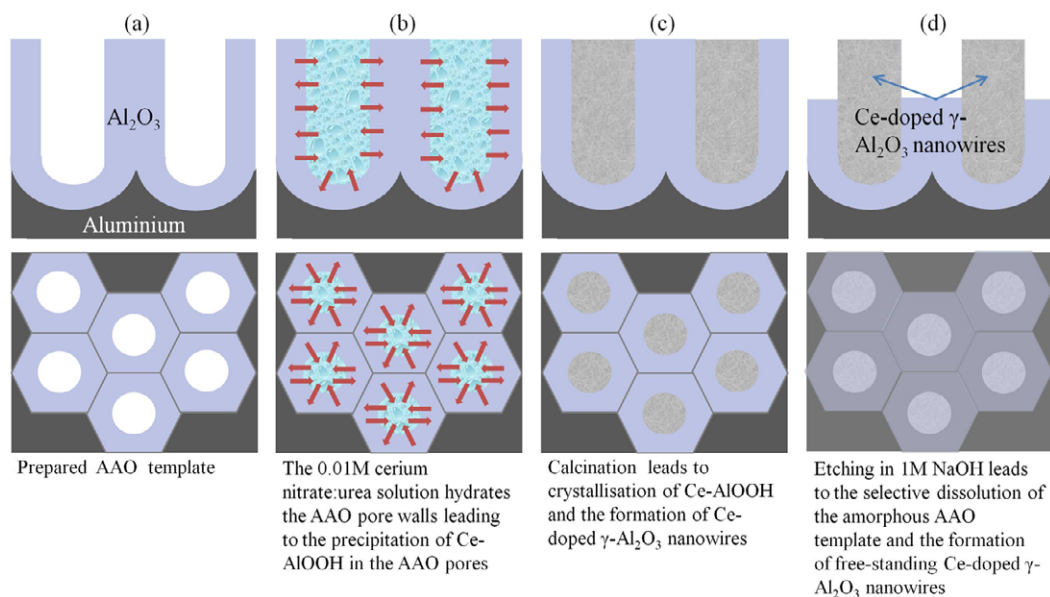


Figure 10. Plan view and cross-section schematic representations of the formation of Ce-doped γ - Al_2O_3 nanowires; (a) prepared AAO templates; (b) immersion of the AAO template in 0.01 M cerium nitrate:urea solution (1:40 molar ratio) leads to hydration of the amorphous Al_2O_3 pore walls which upon saturation results in formation of Ce-containing aluminium oxy-hydroxide (AIOOH) and pore sealing; (c) calcination allows crystallization of Ce-AIOOH to Ce-doped γ - Al_2O_3 ; (d) selective dissolution of the amorphous AAO allows formation of free-standing Ce-doped γ - Al_2O_3 nanowires.

4.6. Possible applications of Ce-doped γ - Al_2O_3

Most industrial catalysts consist of active centres anchored on transition aluminas due to the high porosity, surface area, mechanical strength and thermal stability at moderate temperatures. At high temperature catalytic reactions (1000–1400 °C) the transition from γ - Al_2O_3 to α - Al_2O_3 leads to a considerable reduction of the surface area causing degeneration of the catalytic activity. Various works have established the dependency between the transition temperature of alumina and the surface area retention with the ionic size of the rare earth dopant [1, 2, 4]. Kumar *et al* [4] demonstrated that alumina containing predominantly Ce^{3+} (ionic radius 1.034 Å) exhibits a higher surface area and transformation temperature compared to Ce^{4+} (ionic radius 0.92 Å). The differential scanning calorimetry (DSC) transformation temperature corresponding to the transition to α - Al_2O_3 increased by 100 °C in the case of Ce^{3+} -doped γ - Al_2O_3 . Hence, it should be expected that Ce^{3+} -doped γ - Al_2O_3 nanowires can be utilized as a stable catalyst support for high temperature catalytic reactions.

Finally, the application of post-treatments on nanowires can lead to a number of metal and precious metal supported catalysts via impregnation methods (e.g Rh, Pt, Fe supported on Ce-doped γ - Al_2O_3 nanowires). Ce-doped alumina nanowires (support) can be decorated with a suitable active metal phase which can enhance industrially important reactions. An example of such a family of reactions is the steam reforming of aliphatic and aromatic molecules, used in the purification of gas streams and hydrogen production. It has been shown that these reactions can be facilitated by Ce-doped alumina (in the form of powder) supported Fe catalysts [39].

5. Conclusions

- A novel sol-gel/hydrothermal method has been employed to synthesize Ce-doped γ - Al_2O_3 nanowires. The nanowires have been synthesized in an AAO template via a method involving a 0.01 M cerium nitrate:urea solution at a molar ratio of 1:40 followed by calcination at 500 °C for 5 h. The nanowires were up to tens of microns in length, with diameters of 50–70 nm and exhibited a γ - Al_2O_3 grain size of 2–3 nm. Ce was incorporated within the nanowire in a 3+ oxidation state and was present at a concentration of <1 at.%.
- The chemical processes leading to the formation of Ce-doped γ - Al_2O_3 nanowires have been fully described. Hydrothermal pore sealing of the cerium nitrate sol solution leads to the formation of Ce-doped AIOOH, which, upon calcination, is transformed into Ce-doped γ - Al_2O_3 . Etching in 1 M NaOH preferentially dissolves the amorphous anodic alumina template leaving free-standing Ce-doped γ - Al_2O_3 nanowires.
- A nanocrystalline CeO_2 thin film was also deposited on top of the AAO template. This layer had a cubic fluorite structure and average grain size 6–7 nm.
- With γ - Al_2O_3 being one of the most important alumina phases for catalytic applications, the synthesized Ce-doped nanowires are expected to have improved novel properties and potential applications in catalysis.

Acknowledgments

The authors would like to sincerely thank the Cyprus Research Promotion Foundation for funding this research under Cyprus–France Bilateral Project, No. Cy-Fr0907/2007 (Acronym:

NanoSens) and the European Commission FP6 Marie Curie Actions, Project EXT-0023899 (Acronym: *NanoHeaters*). Dr Kostas Giannakopoulos, Institute of Materials Science, NCSR Demokritos, Greece, is also gratefully acknowledged for his contribution to the electron microscopy work.

References

- [1] Ozawa M, Kimura M and Isogai A 1990 Thermal stability and characterisation of γ -Al₂O₃ modified with rare earths *J. Less-Common Met.* **162** 297
- [2] Kumar K N P, Tranto J, Kumar J and Engell J E 1996 Pore-structure stability and phase transformation in pure and M-doped (M = La, Ce, Nd, Gd, Cu, Fe) alumina membranes and catalyst supports *Mater. Sci. Lett.* **15** 266
- [3] Wei Q, Chen Z-X, Wang Z-H, Hao Y-L, Zou J-X and Nie Z-R 2005 Effect of La, Ce, Y and B addition on thermal stability of unsupported alumina membranes *J. Alloys Compounds* **387** 292
- [4] Kumar K-N-P, Tranto J, Nair B N, Kumar J, Høj J W and Engell J E 1994 Effect of sintering atmosphere on the pore-structure stability of cerium doped nanostructured alumina *Mater. Res. Bull.* **29** 551
- [5] Polychronopoulou K, Fierro J L G and Efstathiou A M 2004 The phenol steam reforming reaction over MgO-based supported Rh catalysts *J. Catal.* **28** 417
- [6] Polychronopoulou K, Costa C N and Efstathiou A M 2004 The steam reforming of phenol reaction over supported-Rh catalysts *Appl. Catal. A* **272** 37
- [7] Steele B C H 1999 Fuel-cell technology—running on natural gas *Nature* **400** 619
- [8] Corma A, Atienzar P, García H and Chane-Ching J-Y 2004 Hierarchically mesostructured doped CeO₂ with potential for solar-cell use *Nat. Mater.* **3** 394
- [9] Masui T, Yamamoto M, Sakata T, Mori H and Adachi G 2000 Synthesis of BN-coated CeO₂ fine powder as a new UV blocking material *J. Mater. Chem.* **10** 353
- [10] Jasinski P, Suzuki T and Anderson H U 2003 Nanocrystalline undoped ceria oxygen sensor *Sensors Actuators B* **95** 73
- [11] Schem M et al 2009 CeO₂-filled sol-gel coatings for corrosion protection of AA2024-T3 aluminium alloy *Corros. Sci.* **51** 2304
- [12] Hutleen J C and Martin C R 1997 A general template-based method for the preparation of nanomaterials *J. Mater. Chem.* **7** 1075
- [13] Kuang D, Fang Y, Liu H, Frommen C and Fenske D 2003 Fabrication of boehmite AlOOH and γ -Al₂O₃ nanotubes via a soft solution route *J. Mater. Chem.* **13** 660
- [14] Hou H, Xie Y, Yang Q, Guo Q and Tan C 2005 Preparation and characterization of γ -AlOOH nanotubes and nanorods *Nanotechnology* **16** 741
- [15] Zhang J et al 2006 Self-assembly of flower-like AlOOH (boehmite) 3D nanostructures *J. Phys. Chem. B* **110** 14249
- [16] Lu C L, Lv J G, Xu L, Guo X F, Hou W F, Hu Y and Huang H 2009 Crystalline nanotubes of γ -AlOOH and γ -Al₂O₃: hydrothermal synthesis, formation mechanism and catalytic performance *Nanotechnology* **20** 215604
- [17] Xiao Z L, Han C Y, Welp U, Wang H H, Kwok W K, Willing G A, Hiller J M, Cook R E, Miller D J and Crabtree G W 2002 Fabrication of alumina nanotubes and nanowires by etching porous alumina membranes *Nano Lett.* **2** 1293
- [18] Tian Y T, Meng G W, Gao T, Sun S H, Xie T, Peng X S, Ye C H and Zhang L D 2004 Alumina nanowire arrays standing on a porous anodic alumina membrane *Nanotechnology* **15** 189
- [19] Sun X X, Liang J, Zhao J F, Ma Q and Xu B S 2010 Preparation of alumina nanowires, nanorods and nanowalls by chemical etching *Appl. Phys. A* **98** 263
- [20] Jha H, Kikuchi T, Sakairi M and Takahashi H 2008 Synthesis of aluminium oxy-hydroxide nanofibers from porous anodic alumina *Nanotechnology* **19** 395603
- [21] Patermarakis G and Kerassovitou P 1992 Study on the mechanism of oxide hydration and oxide pore closure during hydrothermal treatment of porous of porous anodic Al₂O₃ films *Electrochim. Acta* **37** 125
- [22] Patermarakis G, Moussoutzanis K and Chandrinis J 1999 Preparation of ultra-active alumina of designed porous structure by successive hydrothermal and thermal treatments of porous anodic Al₂O₃ films *Appl. Catal. A* **180** 345
- [23] Keijser Th H de, Mittemeijer E J and Rozendaal H C F 1983 The determination of crystallite-size and lattice-strain parameters in conjunction with the profile-refinement method for the determination of crystal structures *J. Appl. Crystallogr.* **16** 309
- [24] Czerwinski F and Szpunar J A 1997 The nanocrystalline ceria sol-gel coatings for high temperature applications *J. Sol-Gel Sci. Technol.* **9** 103
- [25] Ardelean H, Frateur I and Marcus P 2008 Corrosion protection of magnesium alloys by cerium, zirconium and niobium-based conversion coatings *Corros. Sci.* **50** 1907
- [26] Rao M V R and Shripathi T 1997 Photoelectron spectroscopic study of x-ray induced reduction of CeO₂ *J. Electron Spectrosc. Relat. Phenom.* **87** 121
- [27] Yan L, Xing X, Yu R, Deng J, Chen J and Liu G 2007 Facile alcoholthermal synthesis of large scale ceria nanowires with organic surfactant assistance *Physica B* **390** 59
- [28] Garvie L A J and Buseck P R 1999 Determination of Ce⁴⁺/Ce³⁺ in electron-beam-damaged CeO₂ by electron energy-loss spectroscopy *J. Phys. Chem. Solids* **60** 1943
- [29] Garvie L A G, Xub H, Wang Y and Putnam R L 2005 Synthesis of (Ca, Ce³⁺, Ce⁴⁺)₂Ti₂O₇: a pyrochlore with mixed-valence cerium *J. Phys. Chem. Solids* **66** 902
- [30] Xu H and Wang Y 1999 Electron energy-loss spectroscopy (EELS) study of oxidation states of Ce and U in pyrochlore and uraninite ± natural analogues for Pu- and U-bearing waste forms *J. Nucl. Mater.* **265** 117
- [31] Mullejans H and French R H 1996 *J. Phys. D: Appl. Phys.* **29** 1751-60
- [32] Wu G S, Xie T, Yuan X Y, Cheng B C and Zhang L D 2004 An improved sol-gel template synthetic route to large-scale CeO₂ nanowires *Mater. Res. Bull.* **39** 1023-8
- [33] Thompson G E 1997 Porous anodic alumina: fabrication, characterization and applications *Thin Solid Films* **297** 192
- [34] Yakovleva N M, Anicai L, Yakovlev A N, Dima L, Khanina E Ya, Buda M and Chupakhina E A 2002 Structural study of anodic films formed on aluminum in nitric acid electrolyte *Thin Solid Films* **416** 16
- [35] Adachi-Pagano M, Forano C and Besse J-P 2003 Synthesis of Al-rich hydrotalcite-like compounds by using urea hydrolysis reaction-control of size and morphology *J. Mater. Chem.* **13** 1988
- [36] Bokhimi X, Sánchez-Valente J and Pedraza F 2002 Crystallisation of sol-gel boehmite via hydrothermal annealing *J. Solid State Chem.* **166** 182
- [37] Kaplyanskii A A, Kulinkin A B, Kutsenko A B, Feofilov S P, Zakharchenya R I and Vasilevskaya T N 1998 Optical spectra of triply-charged rare-earth ions in polycrystalline corundum *Phys. Solid State* **40** 1310
- [38] Mardilovich P P, Govyadinoy A N, Mazurenko N I and Paterson R 1998 New and modified anodic alumina membranes part II—comparison of solubility of amorphous (normal) and polycrystalline anodic alumina membranes *J. Membr. Sci.* **98** 143
- [39] Polychronopoulou K, Bakandritsos A, Tzitzios V, Fierro J L G and Efstathiou A M 2006 Absorption-enhanced reforming of phenol by steam over supported Fe catalysts *J. Catal.* **241** 132